Insights into complex nanopillar-bacteria interactions: Roles of nanotopography and bacterial surface proteins

Mohd I. Ishak[1,2,3], J. Jenkins[1], S. Kulkarni[4], T.F. Keller[4,5], Wuge H. Briscoe[2], Angela H. Nobbs[1], and Bo Su[1]*

1. Bristol Dental School, University of Bristol, Lower Maudlin Street, Bristol, BS1 2LY, UK

2. School of Chemistry, University of Bristol, Cantock's Close, Bristol BS8 1TS, UK

3. Faculty of Engineering Technology, Universiti Malaysia Perlis (UniMAP), Perlis, Malaysia

4. Deutsches Elektronen-Synchrotron DESY, Notkestraße 85, Hamburg 22607, Germany

5. Physics Department, University of Hamburg, Hamburg, Germany

*Corresponding author. Email: b.su@bristol.ac.uk

Highlights

- Pressure from nanopillars is insufficient to cause damage to bacterial cell envelope.
- Bacteria can regulate the cell envelope stresses caused by the nanopillars.
- Three deformations of bacterial cell envelope were observed: flat; inward and outward.

TOC

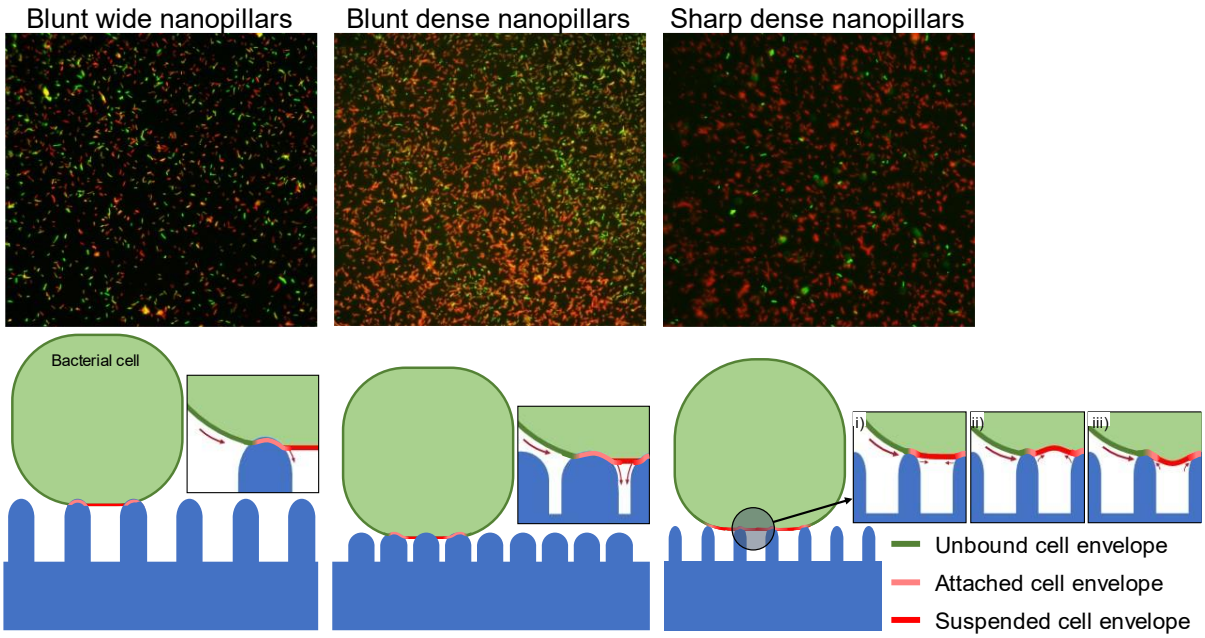

ABSTRACT

Nanopillared surfaces have emerged as a promising strategy to combat bacterial infections on medical devices. However, the mechanisms that underpin nanopillar-induced rupture of the bacterial cell membrane remain speculative. In this study, we have tested three medically relevant poly(ethylene terephthalate) (PET) nanopillared-surfaces with well-defined nanotopographies against both Gram-negative and Gram-positive bacteria. Focused ion beam

scanning electron microscopy (FIB-SEM) and contact mechanics analysis were utilised to understand the nanobiophysical response of the bacterial cell envelope to a single nanopillar. Given their importance to bacterial adhesion, the contribution of bacterial surface proteins to nanotopography-mediated cell envelope damage was also investigated. We found that, whilst cell envelope deformation was affected by the nanopillar tip diameter, the nanopillar density affected bacterial metabolic activities. Moreover, three different types of bacterial cell envelope deformation were observed upon contact of bacteria with the nanopillared surfaces. These were attributed to bacterial responses to cell wall stresses resulting from the high intrinsic pressure caused by the engagement of nanopillars by bacterial surface proteins. Such influences of bacterial surface proteins on the antibacterial action of nanopillars have not been previously reported. Our findings will be valuable to the improved design and fabrication of effective antibacterial surfaces.

Keywords: Nanopillars, Antibacterial, Cell envelope stress, Contact mechanics, Intrinsic pressure, Deformation, Surface proteins

1 Introduction

Utilising nanopillared surfaces as a novel method to combat bacterial infections on medical devices has gained significant interest in recent years, owing to their ability to kill bacteria without the application of antimicrobial agents. Several models and theories have been proposed to understand such bacteria-substrata interactions [1]–[10]. Many of these are based on the assumption that the antibacterial mechanisms of nanopillared surfaces arise from stretching and rupturing of the bacterial cell envelope. More recently, however, antibacterial

effects of nanopillars have been shown to extend to cell entrapment and impairment of biological processes at the molecular level [8]. Current understanding of the specific forces that mediate nanopillar-induced rupture of bacterial cells is still speculative [10]. It has been proposed that mechanobactericidal surfaces induce a self-driven membrane rupture [11]. Alternative suggestions point to the effects of shear forces on motile bacteria [7] or the stored bending energy in flexible high aspect ratio nanopillars [12]. More recently it has been suggested that capillary forces are essential to the rapid killing of bacteria [13]. To establish an improved mechanistic understanding of the bactericidal activity of nanopillars, the fundamental question of the underlying forces must be addressed.

In general, bacterial adhesion to a substratum undergoes four specific phases [14]–[16]. Initially, bacteria in aqueous solution can be transported to a solid surface as aerosols [17],[18] or sedimentation [19],[20]. Under static conditions, bacterial mass transport is mostly due to sedimentation while under dynamic conditions, the mass transport is a combination of sedimentation, convection, and diffusion [20],[21]. Under most experimental conditions, bacterial deposition rates onto a surface will eventually reduce to zero, which may be due to successful deposition of cells or establishment of an equilibrium between reversibly adhered and detached bacteria [16]. When bacteria localise at thermodynamically favourable sites, the bacteria must overcome the repulsive forces between the negatively charged substratum surface and the bacterium. This is often facilitated by elongated surface appendages such as pili or fimbriae, which establish long-range and then short-range interactions with the substratum, including van der Waals forces, electrostatic forces, hydrogen bonding, dipole-dipole, ionic and hydrophobic interactions [14],[22],[23]. This first phase establishes a weak and reversible adhesion. The subsequent second phase is characterised by stronger and irreversible adhesion between the cell and the substratum. This interaction is mediated by specific receptor-ligand interactions between bacterial surface proteins and the substratum.

It is also known that bacteria experience nanoscopic cell envelope deformation when attached to a flat substratum due to adhesion force. This deformation is balanced by the counterforces from the viscoelastic bacterial cell envelope and bacterial turgor pressure [16]. For a flat substratum, the nanoscale deformation is generally considered beneficial as it brings molecules from the cytoplasm closer to the substratum to enhance bacterial molecular interactions with substratum components [16]. Several studies have reported that bacterial cells exhibit a specific response upon contact with an abiotic surface. This has been observed on biomaterials [24], nanoparticles [25] and an AFM tip [26]. It has also been proposed that bacteria can localise adhesins to the area of contact to establish stronger adhesion [27],[28]. On a flat surface, this adhesion enhancement mechanism could promote bacterial attachment and subsequent biofilm formation. By contrast, a higher adhesion force on nanopillared surfaces may increase the intrinsic pressure within the bacterial cell on and around the nanopillars, triggering stress responses and/or physical damage [8].

In this study, three interrelated medically relevant polyethylene terephthalate (PET) nanopillared surfaces were utilised to understand the role of bacterial adhesion force, facilitated by bacterial surface proteins, during attachment to nanopillared surfaces and their correlation with antibacterial activity. Our FIB-SEM analysis revealed an adaptive bacterial response when it was exposed to a nanopillared surface, where the bounded region of the cell envelope deformed due to tethering to the nanopillars by bacterial surface proteins. The high intrinsic pressure on the bounded region of the bacterial cell envelope had a detrimental impact on the metabolic activity of the adhered bacteria, but was insufficient to cause catastrophic damage to the bacterial cell envelope. These insights into the interactions between bacteria and nanopillar surfaces, mediated by bacterial surface proteins, serve to inform the rational design of antimicrobial nanopillared surfaces for medical devices.

2 Experimental

2.1 Preparation of nanopillared poly(ethylene terephthalate) (PET) surfaces

The nanofabrication procedure is a two-step process. The first step involves preparation of the master mould using a two-step anodisation technique and the second step involves transfer of the pattern onto the polymer substrate using a hot-embossing technique. Details of both the anodisation and hot-embossing processes are described elsewhere [29]. Briefly, an aluminium foil with a 5 mm thickness (99.9999% purity, Goodfellow) was washed with deionised (DI) water, ethanol (99.6%, Fischer Scientific) and acetone (analytical reagent grade (99.99%), Fisher Scientific) to remove grease before being electropolished in a 1:4 (v/v) perchloric acid (60%, extra pure, Fisher Scientific)/ethanol (analytical reagent grade (99.99%), Fischer Scientific) at 7^{o}C for 2 min at a current density of 0.1 mA mm^{-2}. The first step of anodisation was performed for 4 h followed by removal of the oxide layer in a chromic acid mixture at 50^{o}C for 2 h. The second step anodisation was similar to the first step but with a shorter anodisation time. The detailed anodisation process used to generate different master moulds is summarised in Table S1 in the Supplementary Information (SI) section. The master moulds were treated with dimethyldichlorosilane (DCDMS; (99.5%) 1.6 ml, 5% in heptane (Sigma Aldrich)) to facilitate release of the nanopillars from the anodised aluminium oxide (AAO) mould (Fig. S1).

Next a PET substrate with a 5 mm thickness (99.9%, Goodfellow) was cut into 10×10 mm pieces and cleaned sequentially with *Milli-Q* water (18.2 MΩ cm at 25 °C) and ethanol (analytical reagent grade (99.99%), Fisher Scientific) for 10 min each in an ultrasonic bath at 90% power (100 W) for 10 min. The PET substrate was heated to 90^{o}C before being embossed with the master mould at a pressure of 1.2 MPa for 20 min. The temperature was then cooled to 60^{o}C before the pressure was released. The PET substrate was carefully released from the AAO mould at a wedge angle <10^{o}. All of the nanopillared surfaces were examined using

scanning electron microscopy (SEM) and atomic force microscopy (AFM). SEM images were taken using an FEI Quanta SEM at various magnifications and angles, while AFM images were recorded using a Bruker Multimode III AFM in tapping mode using Si_3N_4 cantilevers (aluminium coated, spring constant: 30 N/m, MikroMasch® Europe). Nanopillared PET samples were sterilised in absolute ethanol, washed in deionised water and dried prior to inoculation with bacterial suspensions.

2.2 Bacterial strains and culture conditions

Escherichia coli strain K12 [30], *Klebsiella pneumoniae* strain IS-2662A (gift from Prof Matthew Avison, University of Bristol) and *Staphylococcus aureus* strain Newman [31] were used in this study. The strains were selected to represent a range of bacteria with different properties, i.e. Gram-type, cell morphology and motility. Bacteria were routinely cultured in Mueller Hinton broth (Sigma-Aldrich) overnight (16 h) at 37ºC, 220 rpm. For use in assays, bacteria were subcultured to OD_{600} 0.1 and grown to mid-exponential phase, before being harvested by centrifugation (5000 rpm, 5 min), washed twice in Tris-HCl buffer (pH 7.0, >99% pure, Sigma-Aldrich) and adjusted in Tris-HCl buffer to OD_{600} 0.5. Mid-exponential phase cultures were selected to ensure that surfaces could be reproducibly inoculated with high numbers of viable, metabolically-active bacteria.

2.3 Determination of antibacterial performance

BacTiter-Glo™ assay (Promega) and BacLight™ LIVE/DEAD assay (L7007, Thermo Fischer Scientific) were used to quantify the antibacterial performance of the nanopillared surfaces. These assays quantify bacterial viability based on independent biological processes; BacTiter-Glo indicates bacterial vitality based on the concentration of ATP while the Live/Dead assay determines bacterial viability based on membrane permeability.

For LIVE/DEAD assays, sterile PET samples were placed inside black 24-well plates (PerkinElmer, MA, USA) and inoculated with 500 μL of bacterial suspension (equivalent to 5×10^5 CFU). Plates were incubated at 37ºC for 3 h under static conditions, after which time the bacterial suspension from each well was discarded and the samples were washed gently by submerging three times in Tris-HCl buffer. LIVE/DEAD stain (3 μL stain in 1 ml of Tris-HCl) was added to each test surface and incubated for 15 min in the dark at room temperature. Samples were then washed with Tris-HCl buffer to remove excess stain and visualised by fluorescence microscopy. A minimum of 5 images using a 20× objective lens were taken randomly per surface, in which green fluorescent bacteria indicated cells with an intact cell membrane while red or orange fluorescent bacteria indicated cells with a compromised cell membrane. Numbers of green or red/orange adherent bacteria were quantified in FIJI software (NIH) using the cell counter batch processing macro.

For BacTiter-Glo assays, sterile PET samples were placed inside white 24-well plates (PerkinElmer, MA, USA) and inoculated with 500 μL of bacterial suspension. Plates were incubated at 37ºC for 3 h under static conditions, after which time the bacterial suspension was removed from each surface and a 20 µl aliquot of this mixed with 20 μL of BacTiter-Glo™ assay reagent (Promega) in a new, white 24-well plate to allow quantification of non-adherent viable cells. The test surfaces were washed gently with Tris-HCl buffer (pH 7.0), transferred to a new, white 24-well plate, and 20 μL of BacTiter-Glo™ reagent was applied to each surface to allow quantification of adherent viable cells. In both instances, plates were incubated for 5 min in the dark prior to relative luminescence unit (RLU) measurement using a Tecan Infinite F200 PRO microplate reader with automatic attenuation and an integration time of 1000 ms and settling time of 0.15 ms.

2.4 SEM and FIB-SEM sample preparation

Bacteria adhered to PET substrates were fixed overnight at 4ºC with 2.5% glutaraldehyde (EM grade, Sigma Aldrich) in 0.1 M sodium cacodylate (98% pure, Acros Organics). Samples were then washed with 0.1 M sodium cacodylate buffer followed by staining steps with thiocarbohydrazide (TCH) (98%, Sigma-Aldrich), 2% OsO_4 (aq) (EM grade Agar Scientific Ltd.), 1% aqueous uranyl acetate (>98%, Fischer Scientific) and 200 μM lead aspartate (0.66% w/v lead nitrate ($\geq$99%, Sigma-Aldrich) added to 0.03 M aspartic acid (>98.5%, Sigma-Aldrich), with the samples washed thoroughly with deionised water after each step. Samples were serially dehydrated with 20%, 40%, 60%, 80% and 100% ethanol (Sigma-Aldrich) for 10 min each before drying using a critical point dryer (Leica CPD300). The dried samples were mounted onto 0.5 inch stubs (Agar Scientific) and sputter coated with gold and palladium for SEM or FIB-SEM characterisation.

2.5 FIB-SEM processes

Samples were loaded into the Scios DualBeam (FEI) chamber and aligned to be perpendicular to the gallium ion beam. The stage was tilted to 52º and bacteria of interest were located using the electron beam with an accelerating voltage of 5 kV and a current of 50 pA before a 500 nm protective platinum layer was deposited onto the bacterium. A rough cut of trenches was milled around the bacterium with a depth of 250 nm using an accelerating voltage of 30 kV and a current of 1 nA. AutoSlice and View software was used to sequentially slice bacteria with a 30 nm thickness for the *E. coli* cells or 20 nm for the *S. aureus* cells. The ion milling was performed with an accelerating voltage of 5 kV and a current of 47.5 pA, and images were acquired using the electron beam with an accelerating voltage of 5 kV and a current of 98 pA.

2.6 FIB-SEM 3D volume rendering

The FIB-SEM data were processed to correct for stage tilt foreshortening and/or vertical shift using the FIB-stack wizard tool in Avizo V9.7 (FEI). Following geometrical corrections, objects of interest (i.e. bacteria and nanopillars) were assigned as different materials in the segmentation editor. The outline of the object was carefully traced from individual orthoslice images. The volume rendering of the object was generated, and the 3D meshes were simplified to <10,000 faces. Smooth surface function was applied to the object to reduce jagged edges of the 3D model. The 3D models were exported in .ply format to be used in other 3D modelling software packages including Blender V2.9 (The Blender Foundation) and Paint 3D (Microsoft Corporation) for recolouring purposes [32].

2.7 Removal of bacterial surface proteins by trypsinisation

Overnight broth cultures of *E. coli* K12 were harvested by centrifugation (5000 x *g*, 7 min) and resuspended to an OD_{600} of 1.6 in either PBS (pH 7.0) for the control group or 0.5% trypsin/EDTA (pH 7.0, Gibco). Suspensions were incubated for 15 min at 37ºC and then cells washed three times with PBS. Cells were resuspended in PBS to OD_{600} 0.5 for hydrophobicity and viability assays or to OD_{600} 1.0 for dynamic light scattering (DLS) experiments.

To confirm the removal of surface proteins by trypsinisation, changes in surface-bound and released protein levels were quantified. Following trypsinisation (or PBS control), cells were harvested by centrifugation (5000 x *g*, 15 min, 4ºC). Supernatants were collected for trichloroacetic acid (TCA) precipitation while the cell pellets were washed three times with PBS and resuspended in deionised water to OD_{600} 1.0. One part volume of ice-cold TCA was added to three parts volume of supernatant and incubated in ice for 60 min to precipitate the protein. Protein was then recovered by centrifugation (14000 x *g*, 15 min, 4ºC), the pellet washed with ice-cold acetone, dried and resuspended in 500 μL of deionised water. Aliquots

(100 μL) of both the cell and released protein suspensions were transferred into Eppendorf tubes and the levels of protein quantified by Lowry assay [33].

2.8 Hydrophobicity assay

Bacterial cell hydrophobicity was evaluated by hexadecane assay [34]. Aliquots (5 ml) of the bacterial suspension were mixed with 500 μL of hexadecane or PBS (control) and incubated for 15 min at room temperature. Changes in OD_{600} before and after this incubation period were used to calculate the percentage of cells that did not adhere to the hydrocarbon. Specifically, the relative hydrophobicity value was calculated using the following formula: $R_{HP} = \left(\frac{OD_{600}\ final}{OD_{600}\ initial}\right)$. Cells are considered relatively hydrophilic when the R_{HP} value is closer to 1 and relatively hydrophobic when R_{HP} is closer to 0.

2.9 Zeta potential measurements

The zeta potential of bacteria and PET substrate was measured using Malvern Zetasizer Nano-ZS (Malvern Panalytical) at pH 7.0. Bacterial suspensions (OD_{600} 1.0) were diluted 1:1000 into Tris-buffer pH 7.0 before being vortexed and transferred onto a capillary zeta cell (DTS1070). All measurements were carried out in triplicate.

2.10 Statistical analysis

All statistical analyses were performed using Microsoft Excel (Microsoft 365). Data were analysed by ANOVA with the Tukey HSD post-hoc test and p-values of <0.05 were considered significant. Unless otherwise stated, data are representative of three experimental replicates (n = 3) performed in triplicate.

3 Results

3.1 Surface characterisation

Three interrelated PET nanopillar designs of uniform height and periodicity were generated to investigate the effects of nanopillar sharpness/curvature and density on their antibacterial activity (Fig. 1): blunt and wide nanopillars (**BWN**) that closely mimic the nanopillars found on *Psaltoda claripennis* wings, which are 70 nm in diameter, 256 nm in height and 122 nm in pitch distance (density of 67 nanopillars per μm^2) [35]; blunt and dense nanopillars (**BDN**) that have the same diameter as BWN but with approximately twice the density (120 nanopillars per μm^2); sharp and dense nanopillars (**SDN**) that have the sharpest nanopillar tip with a diameter of 40 nm but the same density of nanopillars as the BDN surface. The surface roughness, wetting and nanotribological properties of the nanopillared surfaces have been reported in our previous study [29] and are also summarised in Table S2 (Supplementary Information).

3.2 Bacterial membrane susceptibility to nanopillared surfaces

LIVE/DEAD assay was used to determine the capacity for nanopillars to damage the bacterial cell envelope upon adhesion. After 3 hours of static incubation, only 10% of *E. coli* cells and 4% of *K. pneumoniae* cells attached to the flat control PET surface exhibited damaged membranes. In contrast, an estimated 26% of *E. coli* cells and 8% of *K. pneumoniae* cells exhibited compromised cell envelopes on the BWN surface (Fig. 2-3). BDN surfaces had a greater effect on envelope integrity, with 54% of adherent *E. coli* cells and 45% of *K. pneumoniae* cells displaying compromised membranes (Fig. 2-3). The greatest effects on membrane damage were seen for the SDN surface, with damage recorded for 71% of *E. coli* cells and 80% of *K. pneumoniae* cells (Fig. 2-3). By contrast, *S. aureus* cells were minimally affected compared to Gram-negative bacteria. Only 9% and 8% of adherent *S. aureus* cells exhibited membrane permeability on BDN and BWN surfaces, respectively (Fig. 2-3). Again, the highest levels of damage were observed for the SDN surface, but still only reached 15%

(Fig. 2-3). The overall levels of adherent cells differed between the bacterial strains tested, with *K. pneumoniae* exhibiting the highest levels of attachment, but there were no significant differences in the total numbers of adherent cells per area across the different surfaces tested (Fig. 2).

3.3 Effects of nanopillared surfaces on bacterial metabolic activity

Evidence from the literature indicates that bacterial vitality on nanopillared surfaces can be negatively affected, without significant physical damage to the bacteria [36]. Thus, to complement the LIVE/DEAD studies, BacTiter Glo assay was used to assess the vitality of both the adherent bacteria and those in the surrounding suspension following exposure to the different nanopillared surfaces. No significant difference in the numbers of metabolically active adherent cells was observed between the BWN surface and the flat control for any of the three bacterial strains (Fig. 4). By contrast, on the BDN surface, the numbers of metabolically active *E. coli* (Fig. 4A) and *K. pneumoniae* (Fig. 4B) cells were reduced by 39% and 53%, respectively, relative to the control. The SDN surface had the most pronounced effects. Compared to the control, the metabolically active adherent cell populations were reduced by 71%, 60% and 38% for *E. coli* (Fig. 4A), *K. pneumoniae* (Fig. 4B) and *S. aureus* (Fig. 4C), respectively. Of note, for each bacterial strain, there were no significant differences in the numbers of metabolically active cells in the non-adherent cell populations across the different surfaces tested (Fig. 4).

3.4 Effects of nanopillared surfaces on bacterial cell envelope deformation

To assess if there were changes in bacterial morphology that might indicate loss of turgor pressure and to correlate with the measurements of membrane damage, cell envelope deformation for adhered *E. coli* cells was determined using SEM. These studies focused on the SDN surface as this had exhibited the greatest level of bactericidal activity. After reviewing

over 40 images, it was evident that the occurrence of bacterial cells with significant morphological changes or complete deflation was minimal (Fig. S2). The majority of adherent *E. coli* cells displayed the typical bacillus shape and there was evidence that cell surface appendages may facilitate bacterial adhesion to the surface (Fig. 5A). Fig. 5B-D illustrates one of the few examples in which an *E. coli* cell that was fully adsorbed onto the SDN surface displayed a deformation in cell structure. There was evidence of the nanopillars bending towards the cell, which might indicate penetration of the cell by the nanopillars. Thus, the deformation observed may have been due to partial loss of turgor pressure.

To better understand the capacity for the SDN surface to deform the bacterial cell envelope, FIB-SEM was used to perform cross sectional analysis of *E. coli* cells bound to the SDN surface. *S. aureus* was also included to determine if any effects were observed with both Gram-negative and -positive bacteria. Preliminary SEM scanning identified two adherent *E. coli* cells (Fig. 6); one of the cells showed significant deformation (bacterium (i)), while the other cell displayed a typical bacillus shape (bacterium (ii)). Compared to a regular SEM, automated ion beam milling allows visualisation of detailed interactions of the bacterial cell envelope and the nanopillars. Orthoslice data revealed that at least two nanopillars were likely penetrating the deformed bacterium (i), while no such interactions were seen for the seemingly intact bacterium (ii) (Fig. 6A-D). FIB-SEM also indicated stretching of the bacterial cell wall when in contact with the nanopillars (Fig. 6E-G). Three different cell wall conformations were observed: 1) *flat* – no major effects observed, with the suspended bacterial cell envelope appearing flat with no curvature; 2) *inward deformation* - the suspended bacterial cell envelope displayed an inward deformation, pulling away from the nanopillars; and 3) *outward deformation* - the suspended bacterial cell envelope displayed an outward deformation that sank in between the nanopillars.

As for *E. coli*, significant deformation of *S. aureus* cells on the SDN surface was rarely observed, with most of the adherent cells appearing to be suspended on top of the nanopillars and exhibiting a characteristic spherical cell morphology. Nonetheless, data from the LIVE/DEAD and BacTiter Glo assays had indicated the capacity for the SDN surface to reduce *S. aureus* viability relative to the control. Fig. 7 shows a sample in which a total of nine cells were sectioned at 20 nm thickness on the SDN surface, of which four showed signs of deformation. FIB-SEM analysis revealed that the deformed cells were in direct contact with nanopillars, with evidence of cell penetration, again implying that deformation may be due to partial loss of turgor pressure (Fig. 7D). It was also noted that four of the *S. aureus* cells that did not show signs of deformation were not in direct contact with the nanopillars. Rather, these bacteria were in contact with other cells or formed part of a chain with a single cell as the anchor point (Fig. D-E).

3.5 Effects of trypsinisation on *E. coli* surface properties

To investigate the influence of surface proteins on bacterial interactions with nanopillars, *E. coli* cells were trypsinised. Lowry assay was used to confirm the significant release of proteins from the cell surface by this process (Fig. S3). Alongside loss of protein, those remaining proteins that have been cleaved by trypsin will expose a negatively charged carboxylate group [37]. This has the capacity to change the overall surface charge of the cell. As surface charge is a significant factor that can influence bacterial attachment to a substratum, the effects of trypsinisation on this parameter were quantified, alongside hydrophobicity. It was found that untreated (UT) *E. coli* at the mid exponential phase had lower negative zeta potential at ζ = -11.1$\pm$0.7 mV than trypsinised (TRY) *E. coli*, which had a zeta potential of ζ = -16.0$\pm$1.4 mV. TRY *E. coli* cells had a broader zeta potential distribution than UT *E. coli* (Fig. 8A). Similarly, hexadecane assay indicated that the UT *E. coli* cells were significantly more hydrophobic compared to the TRY *E. coli* cells (Fig. 8B).

3.6 Interactions of trypsinised *E. coli* with the SDN surface

To explore how changes in surface protein profile may affect the interactions of *E. coli* with nanopillars, the effects of trypsinisation on *E. coli* attachment to the SDN surface were investigated. *E. coli* cells were incubated with the flat control and the SDN substrata for 3 h, after which metabolic activity of the adhered cells was quantified using BacTiter Glo and the adherent biomass by SYTO9 staining. Trypsinisation did not significantly affect levels of metabolically active *E. coli* cells bound to the flat PET surface (Fig. 9). By contrast, while the levels of metabolic activity were significantly reduced for UT *E. coli* cells on the SDN surface, as expected, no such reduction was seen for the TRY *E. coli* cells. Rather, TRY *E. coli* cells exhibited the levels of metabolic activity that were comparable to those cells bound to the flat surface. No significant differences in biomass were seen across any of the samples tested. SEM images of UT and TRY *E. coli* on the flat and SDN surfaces confirmed that there were no obvious differences in cell morphology caused either by trypsinisation or the nanopillars (Fig. S4).

4 DISCUSSION

Using three well-defined, interrelated nanotopographies, this study set out to better understand how nanopillar dimensions impact the physical response of bacteria, and to explore the potential influence of bacterial surface proteins on this response. As shown in Table S2, both the height and inter-pillar spacing exhibited some variations. It is conceivable that a small fraction of the pillars might not be in contact due to the height polydispersity, leading to a slightly reduced effective pillar density. However, this scenario was not significant due the compliant and deformable bacteria surface. In this study, the nanopillar aspect ratio (AR), rather than height, was controlled to closely mimic cicada wing nanotopographies (Supp Info Table S2). This minimized variations in nanopillar mechanical properties (e.g. stiffness) across the different surface types that might otherwise have influenced their antibacterial properties

[12]. The nanopillars on the BDN surface had the same diameter as those on the BWN surface but were more densely compacted, with an interpillar distance of 100 nm. The increase in the density, *N*, meant that each bacterial cell on the BDN surface interacted with a higher number of nanopillars compared to the BWN surface. According to the model proposed by Li *et al*., this would improve the antibacterial performance compared to the BWN surface [3]. Such effects were seen with *E. coli* and *K. pneumoniae*; a higher percentage of cells bound to the BDN surface exhibited compromised membranes and reduced viability compared to those on the BWN surface. However, this effect was not so clear for *S. aureus*. This suggests that, in contrast to the effects on Gram-negative bacteria, an increase in *N* may not significantly influence the stretching and damage of the Gram-positive cell wall. In recently published work, by systematically tuning polycarbonate nanotopographies, Cui *et al*. reported that nanostructured surfaces with interpillar spacing of 170 nm exhibited higher levels of antibacterial activity against *E. coli* compared to nanostructured surfaces with an interpillar spacing of 100 nm [38]. This apparent discrepancy with the data reported here could be due to the different experimental conditions used for viability assays. The surfaces generated by Cui *et al*. were of similar nanopillar height and cap diameter. In addition, Cui *et al*. suspended the bacteria in 0.85% NaCl while Tris-HCl buffer was used in this study. Changes to physicochemical conditions [39],[40] and the ionic strength [41] are known to have a significant impact on bacterial adhesion to solid substrata.

Previous studies have reported a positive correlation between nanopillar density and bactericidal activity [42],[43], but in most cases no systematic change in the density or nanopillar size was studied. This has made it difficult to identify whether the improvement in bactericidal performance was due to the increase in *N* or the reduction/increase in the tip diameter, D_T. To better understand the relative impact of these parameters here, the SDN surface with similar nanopillar density to the BDN surface but with a much smaller D_T was

designed and tested. The much sharper SDN surface showed the best antibacterial performance of all the nanopillared surfaces tested against Gram-negative bacteria and was the only surface that significantly impaired *S. aureus* viability compared to the control. Thus, this shows that D_T is a parameter that may significantly influence the antibacterial performance of nanopillars, independent of N [44]. Of note, the reduction in metabolic activity of *S. aureus* on the SDN surface was comparable to the levels seen for the Gram-negative cells, while the numbers of *S. aureus* cells with compromised cell membranes were far lower. This implies that the predominant antibacterial effects of nanopillars against *S. aureus* may be attributed to factors such as cell entrapment and induction of oxidative stress [8] rather than cell lysis.

Our 3D reconstruction of the adherent bacteria revealed significant deformation in the bound cell wall region, suggesting localised interactions between the cell wall and the nanopillars (Fig. 10 and Fig. S5). Using the Hertzian model, we estimated the number of nanopillars that would be in contact with a bacterium, the intrinsic contact area, $A_{i,}$ and the intrinsic pressure on a single nanopillar, ρ_i. A detailed explanation for these calculations can be found in Supplementary Information. Briefly, we assumed that bacteria enhanced their adhesion force to individual nanopillars to gain maximum adhesion [26]. Thus, the interacting force, F_i, was assumed to be 20 nN per nanopillar, as reported in the literature [26]. It was found that there were approximately 57 nanopillars in contact with a bacterial cell (size: 1.0 × 0.5 μm) for the BDN and SDN surfaces compared to just 34 nanopillars for the BWN surface. For a nanopillar with a D_T of 80 nm (BDN and BWN), ρ_i on a single nanopillar was around 3.7 MPa, while for a nanopillar with a D_T of 40 nm (SDN), the pressure was $\rho_i \sim 7.0$ MPa. Our semi-quantitative calculation validates our hypothesis that the higher levels of membrane permeabilisation seen for Gram-negative bacteria attached to the BDN surface compared to the BWN surface were due to the higher number of nanopillars that engaged each bacterial cell on the BDN surface, leading to higher stretching of the suspended envelope (Fig. 10A, B). These calculations also

support the theory that blunt nanopillars may not have had sufficient pressure to inflict direct damage on the Gram-negative cell envelope unlike the sharp (SDN) nanopillars (Table S3), as evidenced by the LIVE/DEAD and BacTiter Glo assay data. We attribute the high level of cell permeabilisation seen by LIVE/DEAD assay for *E. coli* and *K. pneumoniae* to cell envelope stress in viable bacteria resulting from nanopillar-induced deformation or to membrane permeabilisation during cell division and cell wall synthesis [36].

Nonetheless, while the FIB-SEM data indicated that the bound cell envelope region of bacteria on the SDN surface experienced the greatest deformation compared to the unbound region, only a few deflated cells were observed implying a lack of lysis. More evidence of deformation of the bound cell envelope region for seemingly healthy bacteria can be found in Fig. S6.These results are consistent with reports that the bacterial cell wall behaves as a viscoelastic solid material [45]–[47] and can be very flexible to ensure survival in unfavourable environments [47],[48]. A recent study also reported a similar observation where the morphology of *P. aeruginosa* cells remained intact when exposed to nanopillared surfaces [13]. They found that an external force was needed to induce morphological changes in the bacteria. Another study [47] found that a pressure of 10.7 MPa was required to puncture the cell wall of *E. coli*, which is higher than previously anticipated (Table S4). Fig. S7 shows a comparison between the pressure needed to puncture the bacterial cell envelope by the nanopillars used in this study and a sharp AFM tip from Valle *et al.* [47]. The range of pressures generated by nanopillars used in this study correspond to the lower number of rupturing occurrences in Valle *et al*. [47]. Taken together, this semi-quantitative comparative analysis corroborates the results of the LIVE/DEAD assay, BacTiter Glo assay and qualitative SEM study and indicates that the majority of bacteria were not susceptible to the biophysical action of the nanopillars, i.e. nanotopography-induced mechanical rupture and cell permeabilisation. Instead, the

predominant antibacterial mechanism of the nanopillars tested here appears to have been associated with induction of changes in bacterial physiology.

The two distinct deformations of the cell envelope (inward and outward deformation) found in this study may be attributed to the surface sensing systems in *E. coli*, one of the key functions of which is to regulate envelope stress [49]. All cell types maintain their membrane integrity to prevent phase transition into a porous state [50]. For instance, it was reported that *E. coli* uses phage shock protein A (PspA) to maintain inner membrane integrity under stress [51]. It was found that PspA has an enhanced sensitivity for stored curvature elastic (SCE) stress and anionic lipids within the membrane. More importantly, PspA was found to control the SCE stress level by enabling nearby lipids to reduce some of the SCE stress to stabilise the membrane. It is possible that the multiple contact points with high pressure per pillar found with our SDN surface caused high levels of SCE stress, requiring the bacterial cell to regulate and stabilise the membrane. The requirement to maintain cell envelope integrity can be anticipated to carry a fitness cost, which could correlate with the reductions seen in bacterial metabolic activity on the SDN surface [8]. The ability of bacteria to regulate membrane stress levels could also explain the unexpected inward envelope deformation observed for many of our samples by FIB-SEM [Fig 6E-G, Fig S6]. It is possible that inward curvature has lower stress than outward curvature, which could explain why inward deformation was observed more frequently. By contrast, the outward deformation could have been caused by tethering of the bacterial cell to nanopillars via its surface proteins. The flat ‘deformation’ found for some samples may indicate the success of the bacterial cell in regulating local SCE stress.

There are several proposed models to identify the potential interactions of bacteria with nanopillared surfaces that induce rupture of the bacterial cell membrane [1]–[3],[5]–[10],[52]. From the proposed theory of bacterial adhesion to substrata [14]–[16],[23], it is expected that

bacterial surface appendages interact with nanopillared surfaces via long- and short-range interactions. This step is crucial for bacteria to penetrate the energy barrier described by the Derjaguin-Landau-Vervey-Overbeek (DLVO) theory to establish adhesion to the substratum. This adhesion will get stronger over time [49], which will promote stretching of the suspended bacterial cell envelope until the stretching limit is reached, leading to cell envelope damage that could potentially lead to rupturing in some cells (Fig. 11A). To study the importance of surface proteins during bacterial adhesion to nanopillared surfaces, *E. coli* cells were treated with trypsin to cleave the surface proteins around the cell. Trypsinisation was used instead of a specific adhesin knockout mutant so as to impact a range of surface proteins simultaneously rather than an individual target. This enabled investigation of the role of bacterial surface proteins more globally. It is well established that *E. coli* uses surface proteins to adhere to substrata [53],[54]. These surface proteins include flagella, type I fimbriae and curli, which have been shown to promote adhesion to abiotic surfaces by breaching the repulsive force on the surface [23],[55],[56]. It was therefore anticipated that trypsinisation may impair the ability of *E. coli* to adhere to nanopillared surfaces since type I fimbriae have been shown to be susceptible to trypsin [53]. Unexpectedly, we found that TRY *E. coli* cells bound at a comparable level to the surfaces as untreated cells but that trypsinisation appeared to render the *E. coli* cells less susceptible to the antibacterial effects of the nanopillars. This suggests that sufficient attractive forces between bacterium and substratum remained following trypsinisation to enable attachment to occur. However, cleavage of surface proteins by trypsinisation may have impaired the strength of the shorter range, irreversible bonds that could form, thereby reducing the overall interaction forces and thus antimicrobial activity of the nanopillars (i.e. cell envelope deformation, stretching, and stress response induction) (Fig. 11B). The extended DLVO theory (XDLVO) proposes that hydrophobic and electrostatic interactions are also important during bacterial adhesion to a substratum, with the former

making the predominant contribution [14]; both parameters are affected by trypsinisation. TRY *E. coli* cells were more negatively charged compared to the untreated cells, meaning that the attractive force of the electrostatic interactions would have been lower for the TRY *E. coli* cells with the negatively charged nanopillared surface. These results corroborate with XDLVO theory, which highlights the importance of bacterial physicochemical properties and surface proteins during complex nanopillar-bacteria interactions.

5 CONCLUSIONS

Several key findings of this study will improve current understanding of bacteria-nanopillar interactions. It was found that bacterial viability was affected by the density of nanopillars, while local deformation of the cell envelope was affected by the intrinsic pressure of the nanopillars, leading to one of three possible modes of cell envelope deformation when suspended between nanopillars: flat, inward or outward. Inward deformation resulted in a much lower stored curvature elastic (SCE) stress compared to the outward deformation, with the latter likely due to tethering of the bacterial cell to the nanopillars via its surface proteins. FIB-SEM data provided important qualitative evidence that deformation of the bound cell envelope region was greater on a surface bearing sharp and dense nanopillars compared to a surface with blunt, wide and sparsely distributed nanopillars. Thus, bacteria in contact with the SDN nanopillars could be expected to have needed to regulate SCE levels caused by the high degree of cell envelope deformation, which may have impaired their overall metabolic activity. Furthermore, by using contact mechanic analysis, we found that the pressure inflicted by a single nanopillar ranged from 3.7 MPa to 7.1 MPa, which was likely insufficient to rupture the Gram-negative bacterial cell envelope. This further supports the proposal that nanopillar-induced cell envelope stress was the principal factor that underpinned the antibacterial properties of our nanopillar surfaces. As such, nanopillared surfaces with high intrinsic pillar pressure per square area can be anticipated to have the most detrimental effects on bacterial

regulation of membrane stress and so exhibit effective antibacterial properties. For future work, other parameters of nanostructured surfaces that can influence bacterial cell envelope stress, like surface wetting, nanotribology, and surface adhesion force need to be considered. Use of proteomics and genomics studies are also essential to fully understand the physiological responses of bacteria to nanopillared surfaces. Overall, understanding the full spectrum of factors that influence the interactions of bacteria with nanopillars will help improve the rational design and fabrication of effective antibacterial surfaces for potential biomedical applications.

CRediT authorship contribution statement

Mohd I. Ishak: Methodology, Validation, Formal analysis, Data Curation, Writing – Original Draft; **Josh Jenkins**: methodology, Data Curation, Writing – Review & Editing; **Satishkumar Kulkarni**: methodology, Data curation, **Thomas F. Keller**: methodology, Resources, Writing – Review & Editing; **Angela Nobbs, Wuge H. Briscoe & Bo Su**: Conceptualization, Resources, Supervision, Writing – Review & Editing, Project administration

Data availability statement

The data is available upon request.

Conflict of Interest

The authors declare no conflict of interest.

Funding Sources

This project is funded by Ministry of Higher Education Malaysia and Universiti Malaysia Perlis through a PhD Scholarship to MII.

Acknowledgments

The authors would like to acknowledge the Ministry of Higher Education Malaysia (MOHE) and Universiti Malaysia Perlis (UniMAP) (SLAB/SLAI2016 Grant) for funding. This research

project has also received funding from the EU H2020 framework programme for research and innovation under grant agreement n. 654360, having benefitted from the access provided by DESY NanoLab in Hamburg (Germany) within the framework of the NFFA Europe Transnational Access Activity.

References

[1] Pogodin, S. *et al.* Biophysical model of bacterial cell interactions with nanopatterned cicada wing surfaces. Biophys. J. **104**, 835–840 (2013).

[2] Xue, F., Liu, J., Guo, L., Zhang, L. & Li, Q. Theoretical study on the bactericidal nature of nanopatterned surfaces. J. Theor. Biol. **385**, 1–7 (2015).

[3] Li, X. & Chen, T. Enhancement and suppression effects of a nanopatterned surface on bacterial adhesion. Phys. Rev. E **93**, 52419 (2016).

[4] Huang, Q. *et al.* Applied Surface Science Enhanced SaOS-2 cell adhesion , proliferation and differentiation on Mg-incorporated micro / nano-topographical TiO 2 coatings. Appl. Surf. Sci. **447**, 767–776 (2018).

[5] Watson, G. S. *et al.* A Simple Model for Binding and Rupture of Bacterial Cells on Nanopillar Surfaces. Adv. Mater. Interfaces **1801646**, 1–8 (2019).

[6] Velic, A., Tesfamichael, T., Li, Z. & Yarlagadda, P. K. D. V. Parametric study on nanopattern bactericidal activity. Procedia Manuf. **30**, 514–521 (2019).

[7] Bandara, C. D. *et al.* Bactericidal Effects of Natural Nanotopography of Dragonfly Wing on *Escherichia coli*. ACS Appl. Mater. Interfaces **9**, 6746–6760 (2017).

[8] Jenkins, J. *et al.* Antibacterial effects of nanopillar surfaces are mediated by cell impedance, penetration and induction of oxidative stress. Nat. Commun. **11**, 1–14 (2020).

[9] Ayazi, M., Ebrahimi, N. G. & Nodoushan, E. J. Bacterial adhesion reduction on the surface with a simulated pattern: An insight into extrand model. Int. J. Adhes. Adhes. **88**, 66–73 (2019).

[10] Ishak, M. I., Liu, X., Jenkins, J., Nobbs, A. H. & Su, B. Protruding Nanostructured Surfaces for Antimicrobial and Osteogenic Titanium Implants. Coatings **10**, 756 (2020).

[11] Elbourne, A. *et al.* Bacterial-nanostructure interactions: The role of cell elasticity and adhesion forces. J. Colloid Interface Sci. **546**, 192–210 (2019).

[12] Linklater, D. P. *et al.* High Aspect Ratio Nanostructures Kill Bacteria via Storage and Release of Mechanical Energy. ACS Nano **12**, 6657–6667 (2018).

[13] Valiei, A. *et al.* Hydrophilic mechano-bactericidal nanopillars require external forces to rapidly kill bacteria. Nano Lett. **20**, 5720–5727 (2020).

[14] Hori, K. & Matsumoto, S. Bacterial adhesion: From mechanism to control. Biochem. Eng. J. **48**, 424–434 (2010).

[15] Berne, C., Ellison, C. K., Ducret, A. & Brun, Y. V. Bacterial adhesion at the single-cell level. Nat. Rev. Microbiol. **16**, 616–627 (2018).

[16] Carniello, V., Peterson, B. W., van der Mei, H. C. & Busscher, H. J. Physico-chemistry from initial bacterial adhesion to surface-programmed biofilm growth. Adv. Colloid Interface Sci. **261**, 1–14 (2018).

[17] Sales-Ortells, H. & Medema, G. Screening-level risk assessment of Coxiella burnetii (Q fever) transmission via aeration of drinking water. Environ. Sci. Technol. **46**, 4125–4133 (2012).

[18] Gut, I. M. *et al.* Extraction of aerosol-deposited *Yersinia pestis* from indoor surfaces to determine bacterial environmental decay. Appl. Environ. Microbiol. **82**, 2809 (2016).

[19] Vu, K., Yang, G., Wang, B., Tawfiq, K. & Chen, G. Bacterial interactions and transport

in geological formation of alumino-silica clays. Colloids Surfaces B Biointerfaces **125**, 45–50 (2015).

[20] Li, J., Busscher, H. J., Norde, W. & Sjollema, J. Analysis of the contribution of sedimentation to bacterial mass transport in a parallel plate flow chamber. Colloids Surfaces B Biointerfaces **84**, 76–81 (2011).

[21] Tran, V. B., Fleiszig, S. M. J., Evans, D. J. & Radke, C. J. Dynamics of flagellum-and pilus-mediated association of *Pseudomonas aeruginosa* with contact lens surfaces. Appl. Environ. Microbiol. **77**, 3644 (2011).

[22] Hetrick, E. M. & Schoenfisch, M. H. Reducing implant-related infections: active release strategies. Chem. Soc. Rev. **35**, 780–789 (2006).

[23] Dufrêne, Y. F. & Persat, A. Mechanomicrobiology: how bacteria sense and respond to forces. Nat. Rev. Microbiol. **18**, 227–240 (2020).

[24] Alam, F. & Balani, K. Adhesion force of *staphylococcus aureus* on various biomaterial surfaces. J. Mech. Behav. Biomed. Mater. **65**, 872–880 (2017).

[25] Zhang, W., Stack, A. G. & Chen, Y. Interaction force measurement between *E. coli* cells and nanoparticles immobilized surfaces by using AFM. Colloids Surfaces B Biointerfaces **82**, 316–324 (2011).

[26] Potthoff, E., Ossola, D., Zambelli, T. & Vorholt, J. A. Bacterial adhesion force quantification by fluidic force microscopy. Nanoscale **7**, 4070–4079 (2015).

[27] Agladze, K., Wang, X. & Romeo, T. Spatial periodicity of *Escherichia coli* K-12 biofilm microstructure initiates during a reversible, polar attachment phase of development and requires the polysaccharide adhesin PGA. J. Bacteriol. **187**, 8237–8246 (2005).

[28] Vissers, T. *et al.* Bacteria as living patchy colloids: Phenotypic heterogeneity in surface adhesion. Sci. Adv. **4**, eaao1170 (2018).

[29] Ishak, M. I., Dobryden, I., Claesson, P. M., Briscoe, W. H. & Su, B. Friction at nanopillared polymer surfaces beyond Amontons' laws: Stick-slip amplitude coefficient (SSAC) and multiparametric nanotribological properties. J. Colloid Interface Sci. (2020).

[30] Hautefort, I., Proença, M. J. & Hinton, J. C. D. Single-copy green fluorescent protein gene fusions allow accurate measurement of Salmonella gene expression in vitro and during infection of mammalian cells. Appl. Environ. Microbiol. **69**, 7480–7491 (2003).

[31] James, E. H., Edwards, A. M. & Wigneshweraraj, S. Transcriptional downregulation of agr expression in *Staphylococcus aureus* during growth in human serum can be overcome by constitutively active mutant forms of the sensor kinase AgrC. FEMS Microbiol. Lett. **349**, 153–162 (2013).

[32] Jenkins, J. *et al.* Resolving physical interactions between bacteria and nanotopographies with focused ion beam scanning electron microscopy. iScience (in press).

[33] Waterborg, J. H. The Lowry method for protein quantitation. in *The protein protocols handbook* 7–10 (Springer, 2009).

[34] Goldberg, S., Doyle, R. J. & Rosenberg, M. Mechanism of enhancement of microbial cell hydrophobicity by cationic polymers. J. Bacteriol. **172**, 5650 (1990).

[35] Ivanova, E. P. *et al.* Natural bactericidal surfaces: mechanical rupture of *Pseudomonas aeruginosa* cells by cicada wings. Small **8**, 2489–2494 (2012).

[36] Stiefel, P., Schmidt-Emrich, S., Maniura-Weber, K. & Ren, Q. Critical aspects of using

bacterial cell viability assays with the fluorophores SYTO9 and propidium iodide. BMC Microbiol. **15**, 36 (2015).

[37] Lee, M. H. & Manoil, C. Engineering trypsin-sensitive sites in a membrane transport protein. Protein Eng. (1997).

[38] Cui, Q., Liu, T., Li, X., Song, K. & Ge, D. Nanopillared Polycarbonate Surfaces Having Variable Feature Parameters as Bactericidal Coatings. ACS Appl. Nano Mater. **3**, 4599–4609 (2020).

[39] Lorite, G. S. *et al.* Surface physicochemical properties at the micro and nano length scales: role on bacterial adhesion and *Xylella fastidiosa* biofilm development. PLoS One **8**, e75247 (2013).

[40] Harimawan, A., Rajasekar, A. & Ting, Y. P. Bacteria attachment to surfaces - AFM force spectroscopy and physicochemical analyses. J. Colloid Interface Sci. **364**, 213–218 (2011).

[41] Zita, A. & Hermansson, M. Effects of ionic strength on bacterial adhesion and stability of flocs in a wastewater activated sludge system. Appl. Environ. Microbiol. **60**, 3041–3048 (1994).

[42] Kelleher, S. M. *et al.* Cicada Wing Surface Topography: An Investigation into the Bactericidal Properties of Nanostructural Features. ACS Appl. Mater. Interfaces **8**, 14966–14974 (2016).

[43] Dickson, M. N., Liang, E. I., Rodriguez, L. A., Vollereaux, N. & Yee, A. F. Nanopatterned polymer surfaces with bactericidal properties. Biointerphases **10**, 021010 (2015).

[44] Hizal, F., Choi, C. H., Busscher, H. J. & Van Der Mei, H. C. Staphylococcal Adhesion, Detachment and Transmission on Nanopillared Si Surfaces. ACS Appl. Mater. Interfaces **8**, 30430–30439 (2016).

[45] Vadillo-Rodriguez, V., Beveridge, T. J. & Dutcher, J. R. Surface viscoelasticity of individual gram-negative bacterial cells measured using atomic force microscopy. J. Bacteriol. **190**, 4225–4232 (2008).

[46] Thwaites, J. J. & Mendelson, N. H. Biomechanics of bacterial walls: studies of bacterial thread made from Bacillus subtilis. Proc. Natl. Acad. Sci. **82**, 2163–2167 (2006).

[47] del Valle, A. *et al.* Mechanically-Induced Bacterial Death Imaged in Real-Time: a Simultaneous Nanoindentation and Fluorescence Microscopy Study. ACS Appl. Mater. Interfaces (2020).

[48] Suo, Z., Avci, R., Deliorman, M., Yang, X. & Pascual, D. W. Bacteria survive multiple puncturings of their cell walls. Langmuir **25**, 4588–4594 (2009).

[49] Sjollema, J. *et al.* Detachment and successive re-attachment of multiple, reversibly-binding tethers result in irreversible bacterial adhesion to surfaces. Sci. Rep. **7**, 1–13 (2017).

[50] Attard, G. S., Templer, R. H., Smith, W. S., Hunt, A. N. & Jackowski, S. Modulation of CTP: phosphocholine cytidylyltransferase by membrane curvature elastic stress. Proc. Natl. Acad. Sci. **97**, 9032–9036 (2000).

[51] McDonald, C., Jovanovic, G., Ces, O. & Buck, M. Membrane stored curvature elastic stress modulates recruitment of maintenance proteins PspA and Vipp1. MBio **6**, (2015).

[52] Wu, S., Zuber, F., Maniura-Weber, K., Brugger, J. & Ren, Q. Nanostructured surface

topographies have an effect on bactericidal activity. J. Nanobiotechnology **16**, 1–9 (2018).

[53] Munera, D., Palomino, C. & Fernández, L. Á. Specific residues in the N-terminal domain of FimH stimulate type 1 fimbriae assembly in *Escherichia coli* following the initial binding of the adhesin to FimD usher. Mol. Microbiol. **69**, 911–925 (2008).

[54] McLay, R. B. *et al.* Level of fimbriation alters the adhesion of *Escherichia coli* bacteria to interfaces. Langmuir **34**, 1133–1142 (2018).

[55] Beloin, C., Roux, A. & Ghigo, J.-M. *Escherichia coli* biofilms. in *Bacterial Biofilms* (ed. Romeo, T.) 249–289 (Springer, 2008).

[56] Francius, G. *et al.* Bacterial surface appendages strongly impact nanomechanical and electrokinetic properties of escherichia coli cells subjected to osmotic stress. PLoS One **6**, 1–18 (2011).

Table and Figure Captions

Fig. 1 Tilted (45º) SEM images of the nanopillared PET surfaces with **(a)** blunt and wide nanopillars (BWN), **(b)** blunt and dense nanopillars (BDN), and **(c)** sharp and dense nanopillars (SDN).

Fig. 2 Quantification of damaged and adherent bacterial cells on control, BWN, BDN or SDN nanopillared surfaces. Suspensions of **(A)** *E. coli*, **(B)** *K. pneumoniae*, or **(C)** *S. aureus* were incubated on the surfaces for 3 h. Following LIVE/DEAD stain, the total number of adherent bacteria per area (blue) and the percentage of adherent cells with a compromised membrane (red) were determined. Data are presented as mean ± SD. *P<0.05 compared to control, as determined by one-way ANOVA with Tukey HSD post-hoc test; n=3.

Fig. 3 Representative fluorescence micrographs of bacteria attached to different nanopillared surfaces. Suspensions of *E. coli* (left column), *K. pneumoniae* (middle column) or *S. aureus* (right column) were incubated on control, BWN, BDN or SDN nanopillared surfaces for 3 h. Following LIVE/DEAD stain, relative proportions of viable (green) or damaged (red/orange) bacteria were visualised and quantified, as indicated by the inset pie chart on each image. Scale bars, 40 μm.

Fig. 4 Quantification of bacterial vitality on control, BWN, BDN or SDN nanopillared surfaces. Suspensions of **(A)** *E. coli*, **(B)** *K. pneumoniae* or **(C)** *S. aureus* were incubated on the surfaces for 3 h. The numbers of metabolically active bacteria were then determined by BacTiter Glo assay for both adherent (grey) and non-adherent (hatched) populations. Data are presented as mean ± SD. *P<0.05 compared to the control, as determined by one-way ANOVA with Tukey HSD post-hoc test; n=3.

Fig. 5 High tilted (80º) SEM images of *E. coli* on flat and SDN surfaces. After 3 h of static incubation at 37ºC, **(A)** *E. coli* cells attached to the flat surface displayed the typical bacillus morphology without any deformation. Surface appendages are marked with red arrows. **(B)** An *E. coli* cell bound to the SDN surface displayed a distorted cell morphology due to potential cell wall damage. Two areas of interest were magnified **(C, D)** and showed several nanopillars that appeared to have penetrated the cell (red circles). White arrows indicate a reduction in the cell volume due to possible loss of turgor pressure.

Fig. 6 FIB-SEM analysis using Avizo V9.0 of *E. coli* cells on the SDN surface. **(A)** SEM image of *E. coli* cells on the SDN surface. **(B)** 3D volume rendering of the cells in **(A)** showing potential regions of the bacterial cell wall i) that were affected by nanopillars (red circles). Red nanopillars indicate those that appear to penetrate the cell wall. **(C, D)** show the orthoslice FIB milling data of the affected cell wall regions indicated in **(B)**. **(E-G)** show three observed deformation modes of nanopillars on the bacterial cell wall: flat **(E)**, inward **(F)** and outward **(G)**.

Fig. 7 SEM images and 3D volume rendering of *S. aureus* cells bound to the SDN surface using Blender 2.8. **(A)** Top view of nine *S. aureus* cells attached to the SDN surface. **(B, C)** Different sections of the milling interface where the cells were coated with a 500 nm thick protective platinum layer prior to ion beam milling. The visible bacteria at each section are marked as SA1 to SA7. **(D)** Analysis following 3D rendering of the sample showed that at least 4 cells (red) were fully adsorbed onto the nanopillars (SA1, SA2, SA3, SA5), while SA6 (purple) was suspended on top of the nanopillars. Four cells (SA4, SA7-9) were not in direct contact with nanopillars (green). **(E)** Clipping mask revealed that SA7-9 formed a chain of cells originating from SA6. Red boxes indicate septa.

Fig. 8 Effects of trypsinisation on *E. coli* K12. **(A)** Zeta potential distribution and **(B)** hydrophobicity of the untreated (UT) (red line) and trypsinised (TRY) (green line) *E. coli* cells. Data are presented as mean ± SD. *P<0.05 compared to the control, as determined by one-way Student's T-test; n=3.s

Fig. 9 Effects of trypsinisation on *E. coli* attachment to flat control or SDN surfaces. Metabolic activity (filled) and total biomass (striped) of untreated (UT) and trypsinised (TRY) *E. coli* cells are shown. Data are presented as mean ± SD. *P<0.05 compared to control, as determined by one-way ANOVA with Tukey HSD post-hoc test; n=3.

Fig. 10 Comparison of bacterial attachment to the nanopillared surfaces and its effects on cell envelope stretching. The cell envelope of bacteria adhered to the nanopillars will have unbound (green) and bound (red and pink) regions that exhibit different stretching behaviours. Within the bound region, the cell envelope that is in contact with the nanopillars (pink) will have lower stretching compared to the cell envelope that is suspended between the nanopillars (red). A bacterial cell that is bound to **(A)** BWN or **(B)** BDN surfaces will have a stretched cell envelope in the unbound region (green line) due to the lower intrinsic contact area compared to the flat

control. **(C)** The unbound region of a bacterial cell bound to the SDN surface will be more stretched compared to the BWN and BDN surfaces due to the smaller intrinsic contact area. The inset on each panel shows the potential cell envelope behaviour when interacting with the nanopillars. As evidenced from FIB-SEM, the suspended cell envelope in the bound region can display one of three different deformations: **(i)** flat, **(ii)** inward or **(iii)** outward.

Fig. 11 Possible mechanism of surface protein-induced, nanotopography-mediated cell envelope damage. **(A)** Stretching of the suspended envelope of untreated *E. coli* cells eventually deforms significantly due to bacterial surface proteins. **(B)** Stretching of the suspended envelope of TRY *E. coli* cells is not significant due to reduced functionality of the surface proteins.

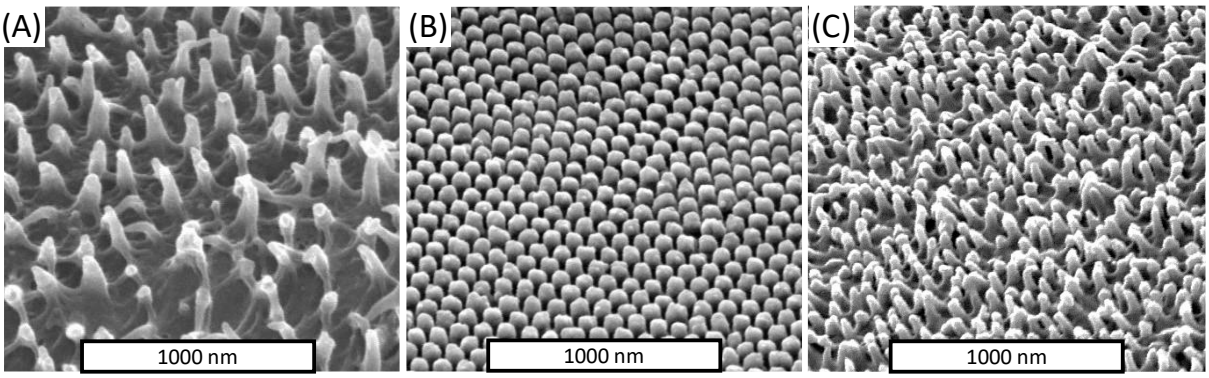

Fig. 1 Tilted (45º) SEM images of the nanopillared PET surfaces with **(a)** blunt and wide nanopillars (BWN), **(b)** blunt and dense nanopillars (BDN), and **(c)** sharp and dense nanopillars (SDN).

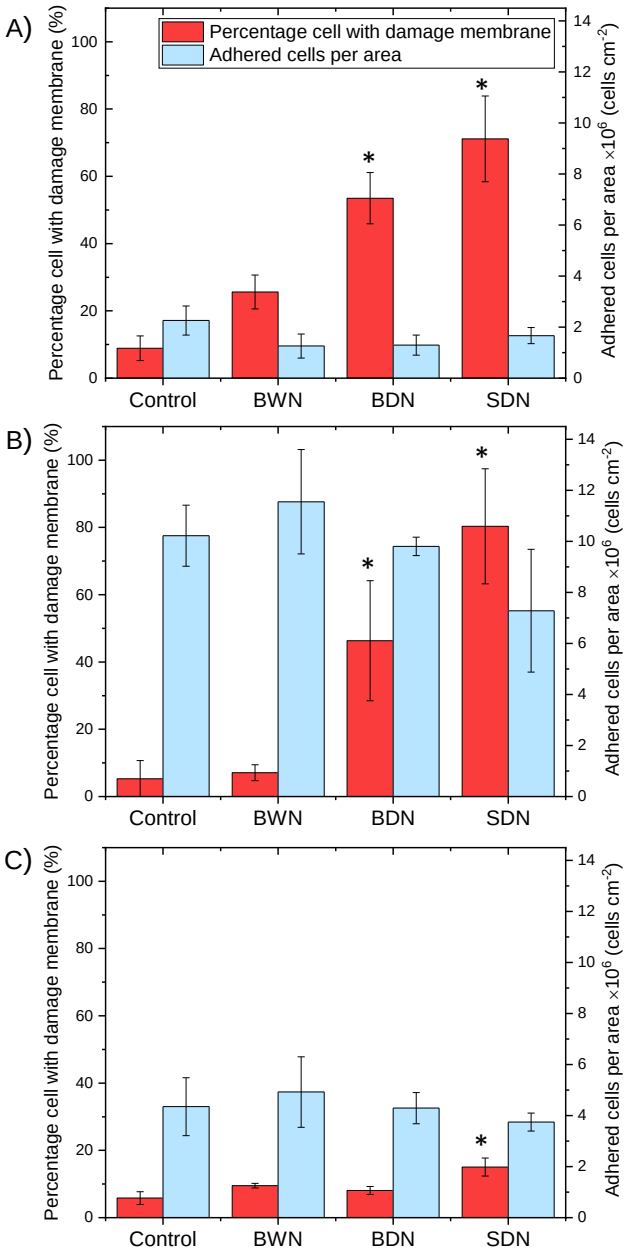

Fig. 2 Quantification of damaged and adherent bacterial cells on control, BWN, BDN or SDN nanopillared surfaces. Suspensions of **(A)** *E. coli*, **(B)** *K. pneumoniae*, or **(C)** *S. aureus* were incubated on the surfaces for 3 h. Following LIVE/DEAD stain, the total number of adherent bacteria per area (blue) and the percentage of adherent cells with a compromised membrane (red) were determined. Data are presented as mean ± SD. *P<0.05 compared to control, as determined by one-way ANOVA with Tukey HSD post-hoc test; n=3.LIVE/DEAD

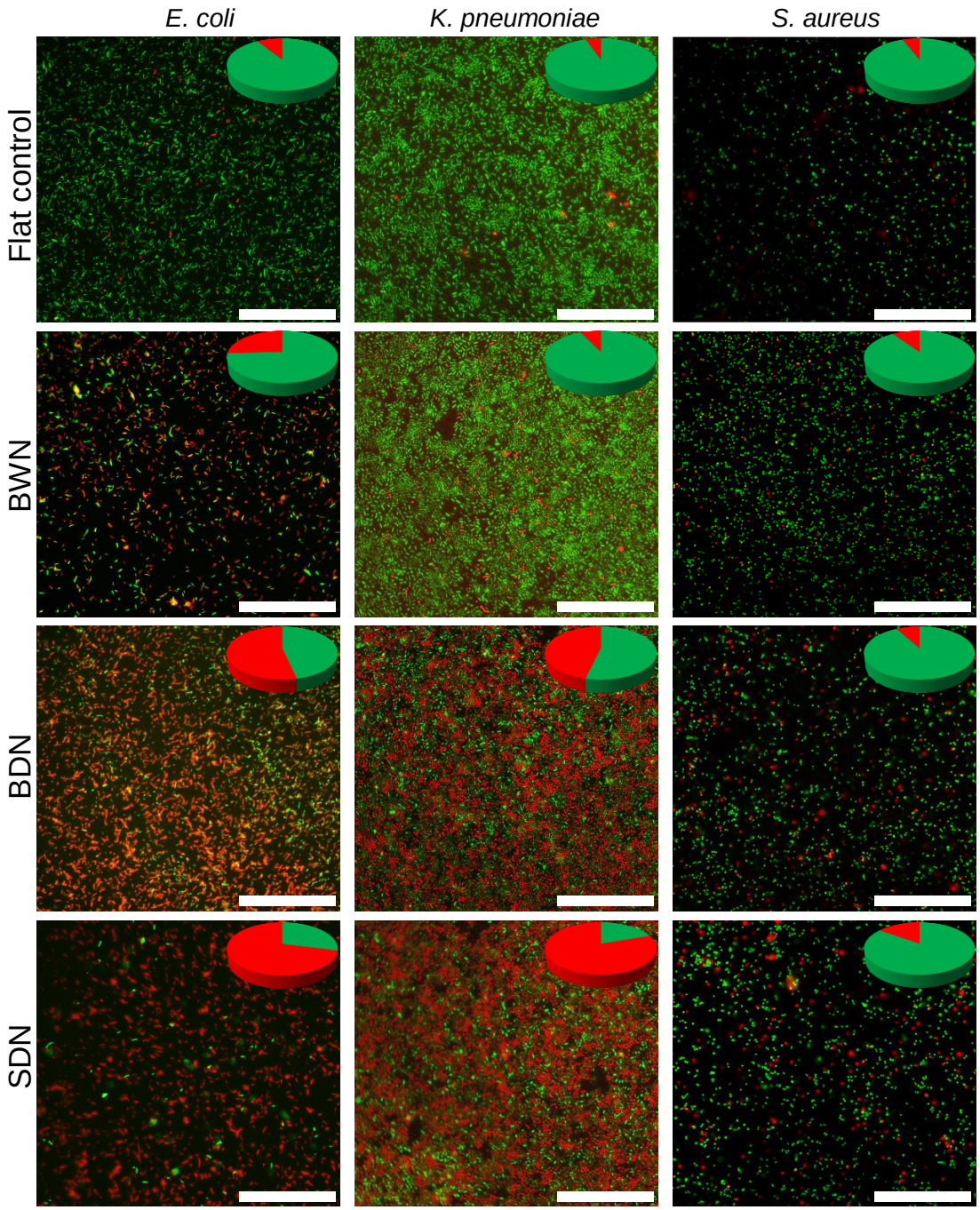

Fig. 3 Representative fluorescence micrographs of bacteria attached to different nanopillared surfaces. Suspensions of *E. coli* (left column), *K. pneumoniae* (middle column) or *S. aureus* (right column) were incubated on control, BWN, BDN or SDN nanopillared surfaces for 3 h. Following LIVE/DEAD stain, relative proportions of viable (green) or damaged (red/orange) bacteria were visualised and quantified, as indicated by the inset pie chart on each image. Pie charts indicate the average values for the representative images. Scale bars, 40 μm. LIVE/DEAD

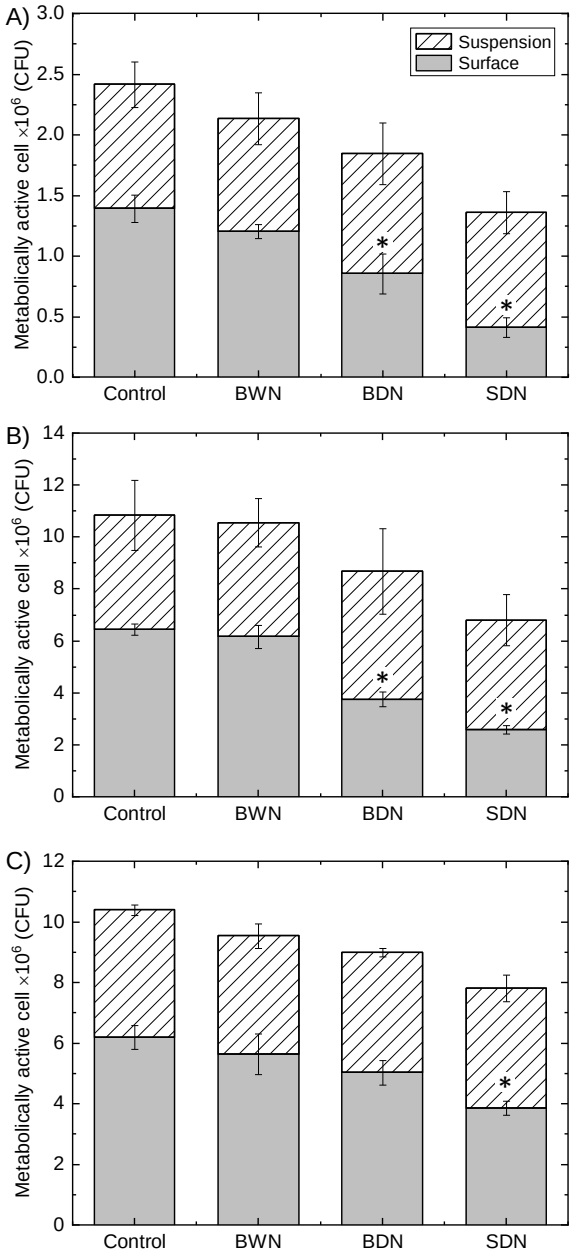

Fig. 4 Quantification of bacterial vitality on control, BWN, BDN or SDN nanopillared surfaces. Suspensions of **(A)** *E. coli*, **(B)** *K. pneumoniae* or **(C)** *S. aureus* were incubated on the surfaces for 3 h. The numbers of metabolically active bacteria were then determined by BacTiter Glo assay for both adherent (grey) and non-adherent (hatched) populations. Data are presented as mean ± SD. *P<0.05 compared to the control, as determined by one-way ANOVA with Tukey HSD post-hoc test; n=3.

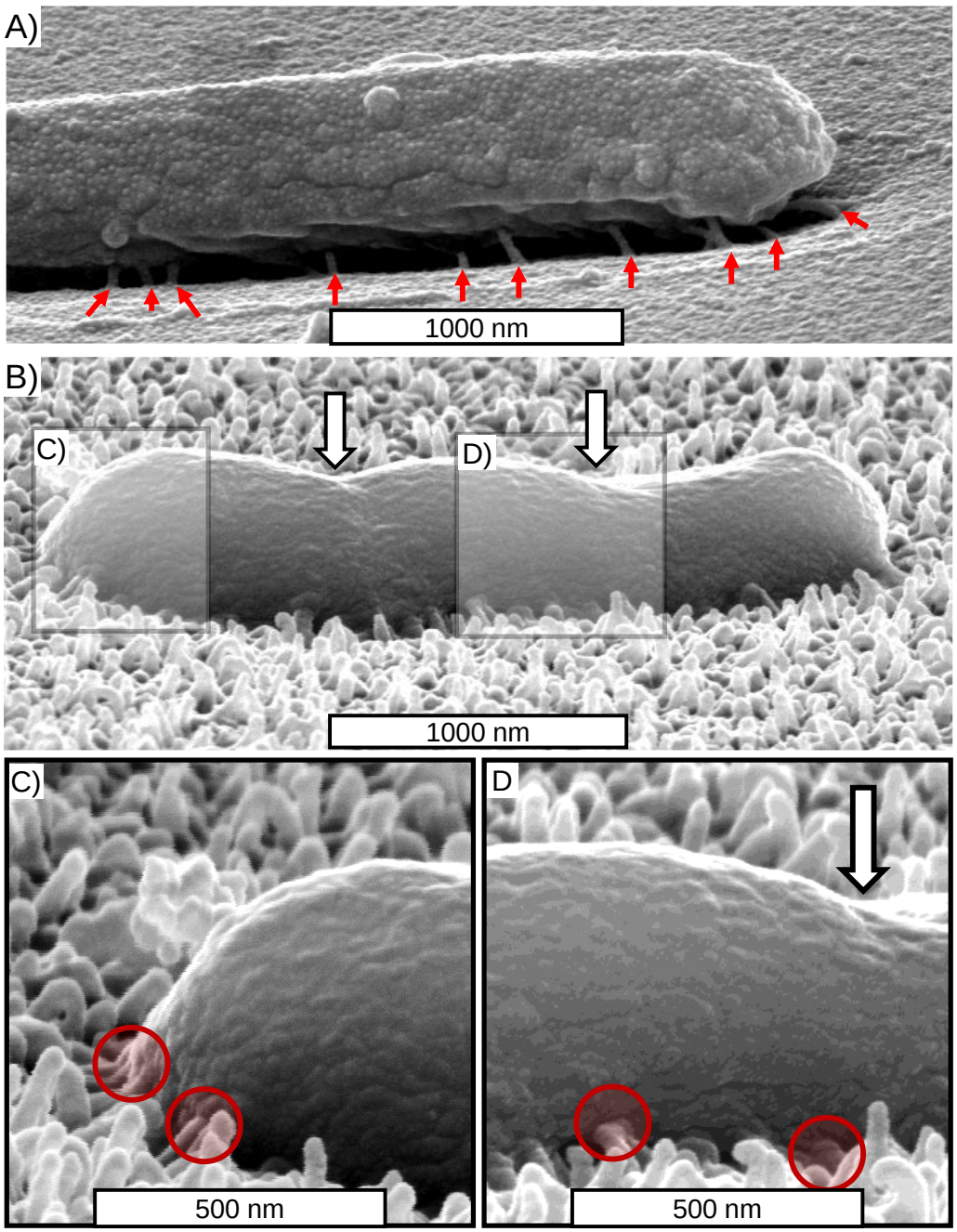

Fig. 5 High tilted (80°) SEM images of *E. coli* on flat and SDN surfaces. After 3 h of static incubation at 37°C, **(A)** *E. coli* cells attached to the flat surface displayed the typical bacillus morphology without any deformation. Surface appendages are marked with red arrows. **(B)** An *E. coli* cell bound to the SDN surface displayed a distorted cell morphology due to potential cell wall damage. Two areas of interest were magnified **(C, D)** and showed several nanopillars that appeared to have penetrated the cell (red circles). White arrows indicate a reduction in the cell volume due to possible loss of turgor pressure.

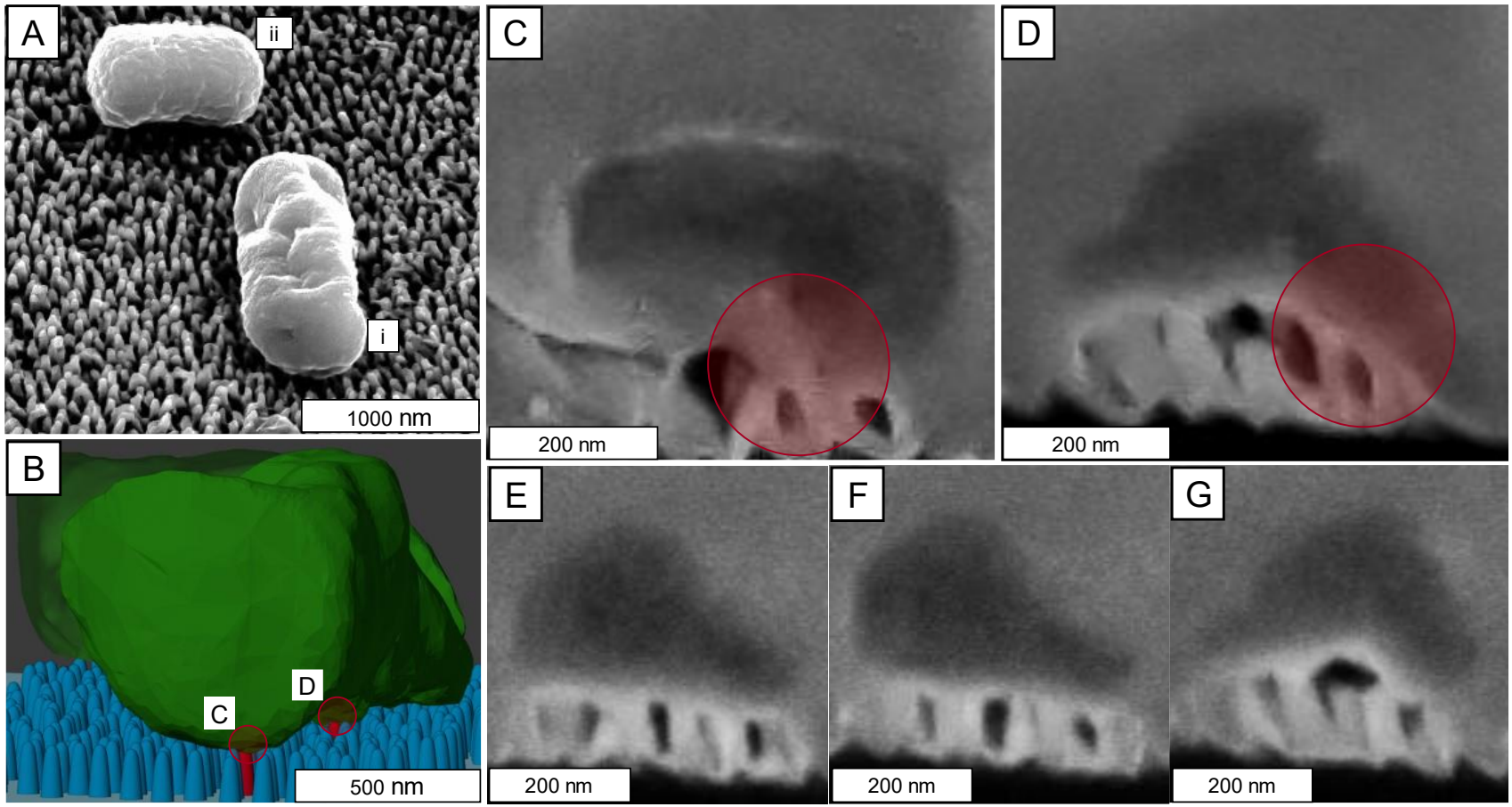

Fig. 6 FIB-SEM analysis using Avizo V9.0 of *E. coli* cells on the SDN surface. **(A)** SEM image of *E. coli* cells on the SDN surface. **(B)** 3D volume rendering of the cells in **(A)** showing potential regions of the bacterial cell wall i) that were affected by nanopillars (red circles). Red nanopillars indicate those that appear to penetrate the cell wall. **(C, D)** show the orthoslice FIB milling data of the affected cell wall regions indicated in **(B)**. **(E-G)** show three observed deformation modes of nanopillars on the bacterial cell wall: flat **(E)**, inward **(F)** and outward **(G)**.

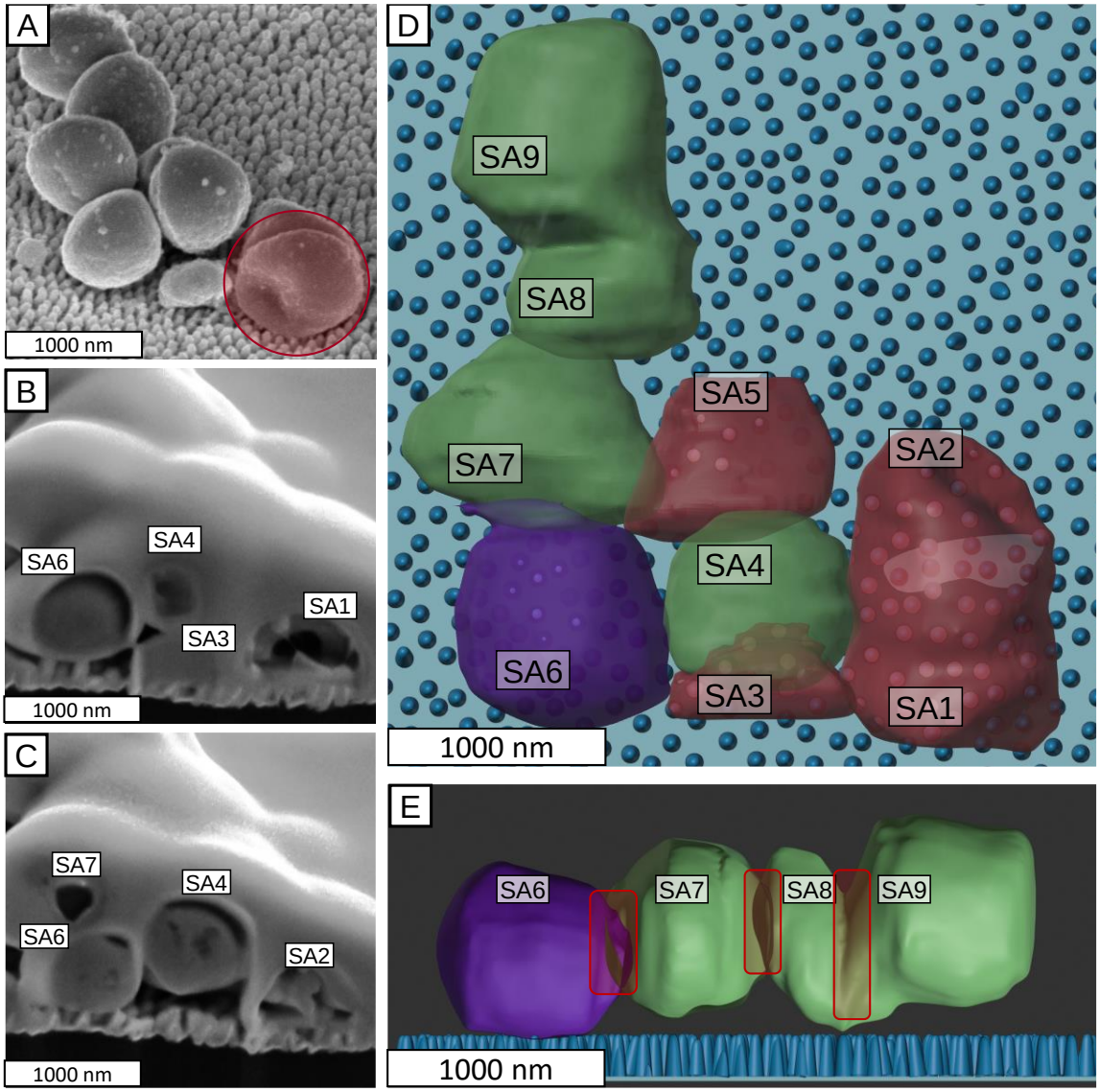

Fig. 7 SEM images and 3D volume rendering of *S. aureus* cells bound to the SDN surface using Blender 2.8. **(A)** Top view of nine *S. aureus* cells attached to the SDN surface. **(B, C)** Different sections of the milling interface where the cells were coated with a 500 nm thick protective platinum layer prior to ion beam milling. The visible bacteria at each section are marked as SA1 to SA7. **(D)** Analysis following 3D rendering of the sample showed that at least 4 cells (red) were fully adsorbed onto the nanopillars (SA1, SA2, SA3, SA5), while SA6 (purple) was suspended on top of the nanopillars. Four cells (SA4, SA7-9) were not in direct contact with nanopillars (green). **(E)** Clipping mask revealed that SA7-9 formed a chain of cells originating from SA6. Red boxes indicate septa.

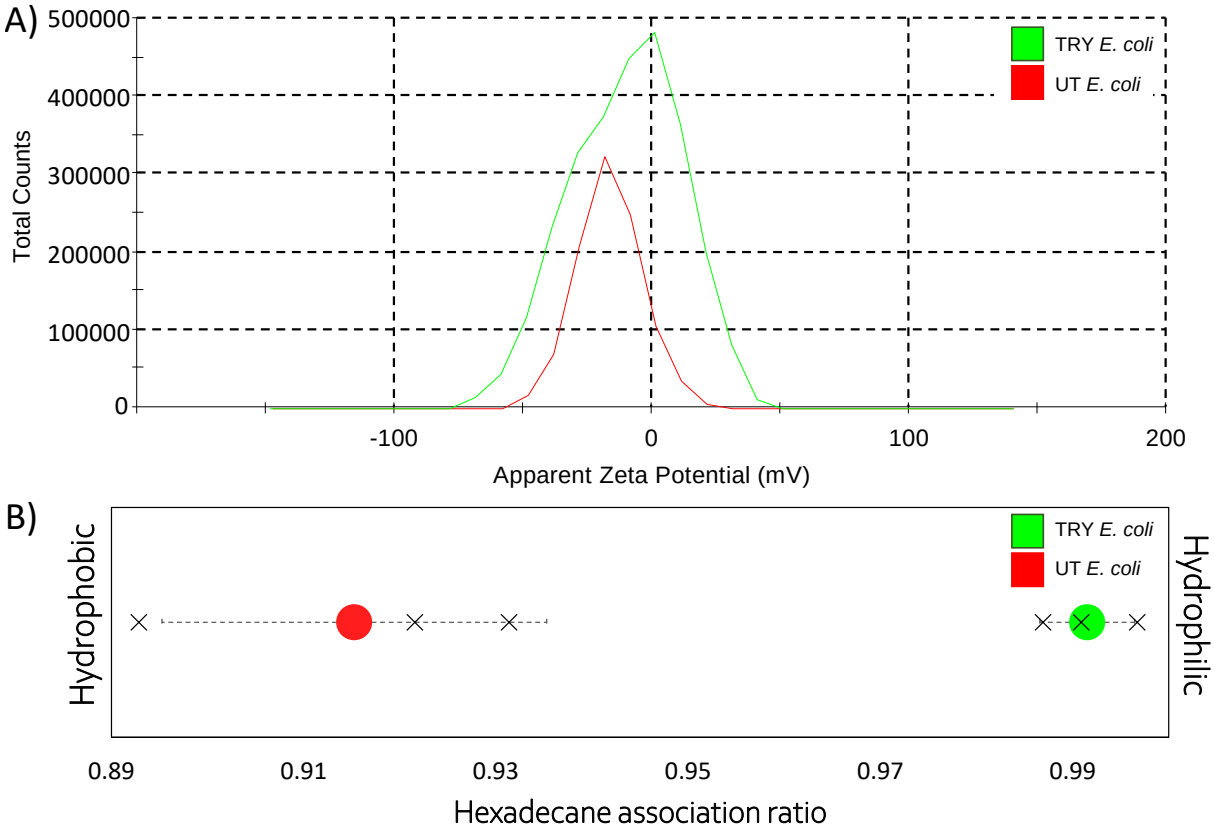

Fig. 8 Effects of trypsinisation on *E. coli* K12. **(A)** Zeta potential distribution and **(B)** hydrophobicity of the untreated (UT) (red line) and trypsinised (TRY) (green line) *E. coli* cells. Data are presented as mean ± SD. *P<0.05 compared to the control, as determined by one-way Student's T-test; n=3.

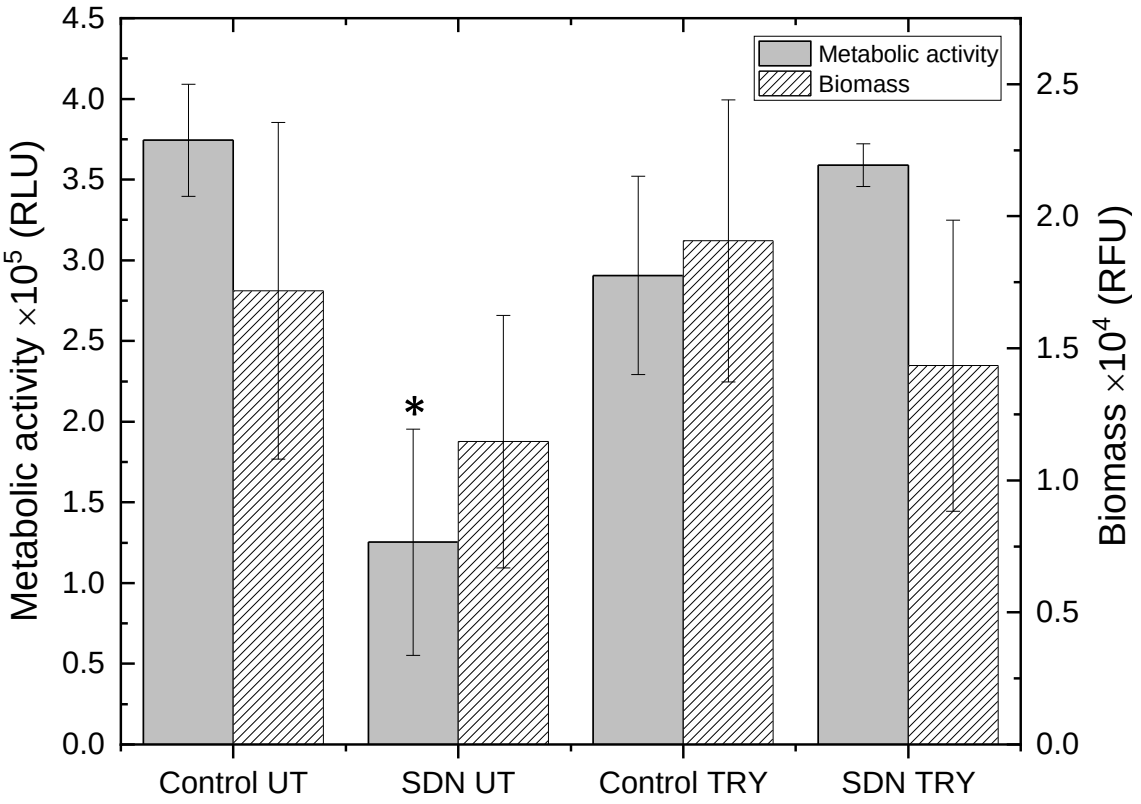

Fig. 9 Effects of trypsinisation on *E. coli* attachment to flat control or SDN surfaces. Metabolic activity (filled) and total biomass (striped) of untreated (UT) and trypsinised (TRY) *E. coli* cells are shown. Data are presented as mean ± SD. *P<0.05 compared to control, as determined by one-way ANOVA with Tukey HSD post-hoc test; n=3.

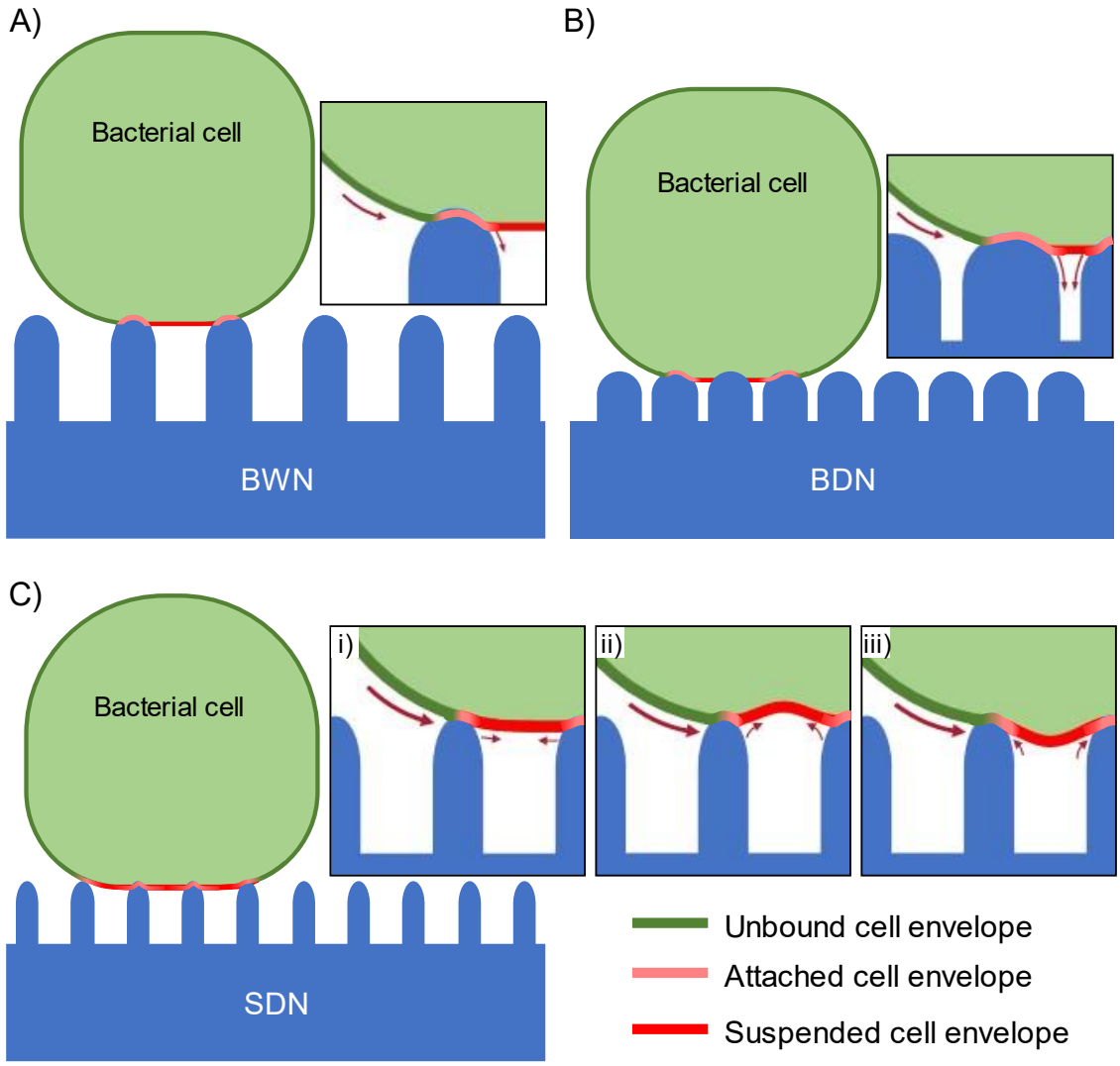

Fig. 10 Comparison of bacterial attachment to the nanopillared surfaces and its effects on cell envelope stretching. The cell envelope of bacteria adhered to the nanopillars will have unbound (green) and bound (red and pink) regions that exhibit different stretching behaviours. Within the bound region, the cell envelope that is in contact with the nanopillars (pink) will have lower stretching compared to the cell envelope that is suspended between the nanopillars (red). A bacterial cell that is bound to **(A)** BWN or **(B)** BDN surfaces will have a stretched cell envelope in the unbound region (green line) due to the lower intrinsic contact area compared to the flat control. **(C)** The unbound region of a bacterial cell bound to the SDN surface will be more stretched compared to the BWN and BDN surfaces due to the smaller intrinsic contact area. The inset on each panel shows the potential cell envelope behaviour

when interacting with the nanopillars. As evidenced from FIB-SEM, the suspended cell envelope in the bound region can display one of three different deformations: **(i)** flat, **(ii)** inward or **(iii)** outward.

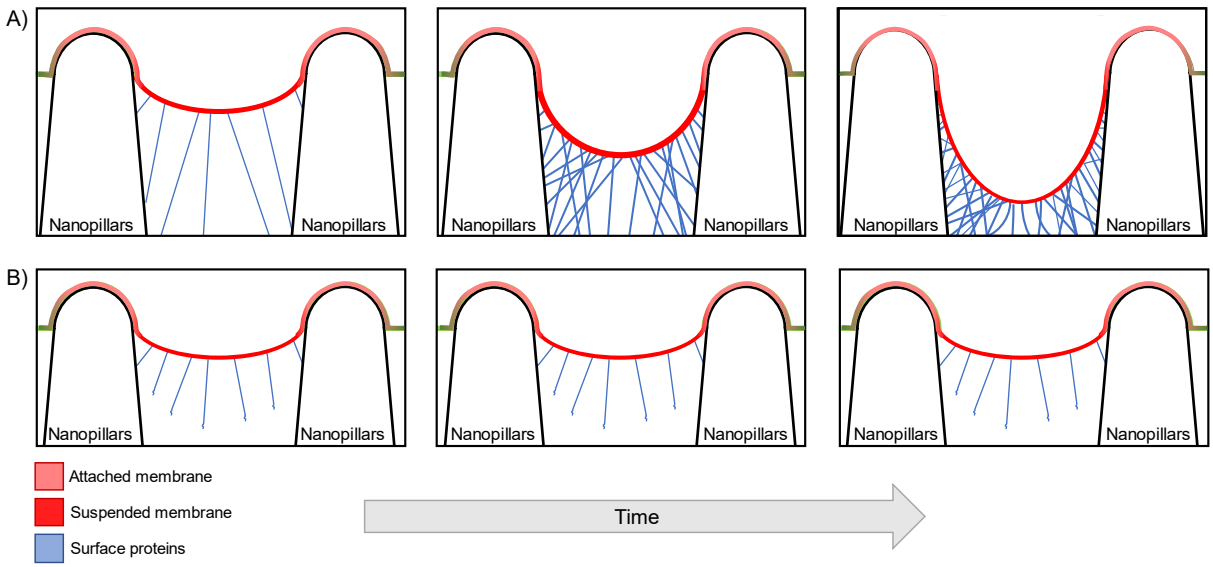

Fig. 11 Possible mechanism of surface protein-induced, nanotopography-mediated cell envelope damage. **(A)** Stretching of the suspended envelope of untreated *E. coli* cells eventually deforms significantly due to bacterial surface proteins. **(B)** Stretching of the suspended envelope of TRY *E. coli* cells is not significant due to reduced functionality of the surface proteins.